Ligament Mediated Fragmentation of Viscoelastic Liquids

Bavand Keshavarz,[1,*] Eric C. Houze,[2] John R. Moore,[2] Michael R. Koerner,[2] and Gareth H. McKinley[1]
[1]Hatsopoulos Microfluids Laboratory, Department of Mechanical Engineering, Massachusetts Institute of Technology, Cambridge, Massachusetts 02139, USA
[2]Axalta Coating Systems, Two Commerce Square, 2001 Market Street, Suite 3600, Philadelphia, Pennsylvania 19103, USA

(Received 6 November 2015; published 7 October 2016)

The breakup and atomization of complex fluids can be markedly different than the analogous processes in a simple Newtonian fluid. Atomization of paint, combustion of fuels containing antimisting agents, as well as physiological processes such as sneezing are common examples in which the atomized liquid contains synthetic or biological macromolecules that result in viscoelastic fluid characteristics. Here, we investigate the ligament-mediated fragmentation dynamics of viscoelastic fluids in three different canonical flows. The size distributions measured in each viscoelastic fragmentation process show a systematic broadening from the Newtonian solvent. In each case, the droplet sizes are well described by Gamma distributions which correspond to a fragmentation-coalescence scenario. We use a prototypical axial step strain experiment together with high-speed video imaging to show that this broadening results from the pronounced change in the corrugated shape of viscoelastic ligaments as they separate from the liquid core. These corrugations saturate in amplitude and the measured distributions for viscoelastic liquids in each process are given by a universal probability density function, corresponding to a Gamma distribution with $n_{\min} = 4$. The breadth of this size distribution for viscoelastic filaments is shown to be constrained by a geometrical limit which can not be exceeded in ligament-mediated fragmentation phenomena.

DOI: 10.1103/PhysRevLett.117.154502

Fragmentation of a viscoelastic jet or sheet is a fundamental component of many industrial and biological processes [1,2]. One important metric of a fragmentation process is the final droplet size distribution, and understanding the role of material properties (e.g., fluid viscosity and relaxation time) on the polydispersity of such distributions is of crucial importance [3,4].

The process of liquid fragmentation has fascinated scientists from ancient [5] to modern times [6–8]. Recent studies [7,9–11] have shown that old paradigms for understanding disintegration of Newtonian liquids, based on either cascade theory [12] (leading to log-normal size distributions) or maximum entropy theories [13] (leading to Poisson size distributions) do not adequately capture all physical aspects of these processes. Villermaux *et al.* [10] show that the atomization process for Newtonian liquids can be precisely described by a fragmentation-coalescence scenario [14]. The final droplet size distribution is a Gamma distribution in which the probability density function (PDF) for a given droplet size [7] is given by

$$p(x = d/\langle d\rangle) = \Gamma(n, x) \equiv [n^n/\Gamma(n)]x^{n-1}e^{-nx}, \quad (1)$$

where $\langle d\rangle$ is the mean or average size [15]. The scale factor n determines how narrow the size distribution is; large values of n indicate a narrow distribution and small values of n describe a broader distribution.

In complex fluids, studies of many capillary-related phenomena have shown interesting and counterintuitive elastic effects [17–19]. However, there is a paucity of fundamental knowledge regarding the dynamics of fragmentation. Experimental studies [20–26] have shown that addition of viscoelasticity can inhibit fragmentation and results in higher values of the average diameter $\langle d\rangle$ for viscoelastic liquid droplets. Keshavarz *et al.* [27] have developed a model predicting the evolution in $\langle d\rangle$ as a function of dimensionless parameters such as the Ohnesorge ($\mathrm{Oh} \equiv \eta/\sqrt{\rho\sigma R_0}$) and Deborah ($\mathrm{De} \equiv \tau_E/\sqrt{\rho R_0^3/\sigma}$) numbers which characterize viscous and elastic effects in the spray process. Here, η is the shear viscosity, σ is the surface tension, and τ_E is the characteristic relaxation time for the viscoelastic liquid. The model predicts a slow, logarithmic growth of $\langle d\rangle$ with De, which agrees with experimental spray measurements. However, none of these studies address the role of viscoelasticity on the distribution of droplet sizes. The few attempts in the literature to address the size distributions for polymeric liquids [28,29] base their assumptions on older paradigms [12,13].

The dramatic change in the inertioelastic breakup of a liquid jet during air-assisted atomization is illustrated in Fig. 1. As previously noted [30], the large scale features remain unchanged, but the addition of a polymer results in finer scale structures such as atomized droplets that remain connected to the core jet by thin viscoelastic ligaments.

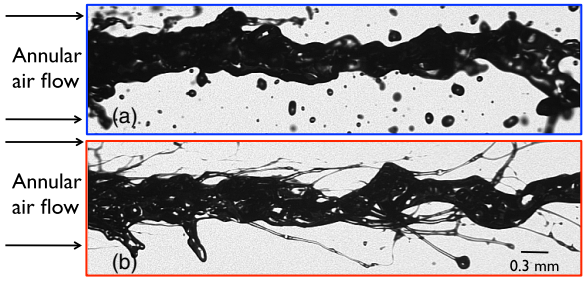

FIG. 1. Snapshot of the liquid jet in the air-assisted atomization for (a) the Newtonian solvent and (b) the viscoelastic solution (PEO-300 K-0.01% wt. in the solvent).

The lifetime of these ligaments depends on the extensional viscosity of the fluid, and it is well known that adding dilute amounts of a high molecular weight flexible macromolecule to a Newtonian solvent will keep the shear viscosity almost unchanged, whereas the extensional viscosity will increase dramatically [31,32].

We have used four different dilute polymeric solutions and three different canonical atomization processes. Table I summarizes the material properties of these fluids.

All four solutions are made by dissolving small amounts of poly(ethylene oxide) (PEO) of different average molecular weights (300 kg/mol and 1000 kg/mol) in a water-glycerol (60%–40% wt.) solvent. The coil overlap concentrations are, respectively, $c^* = 0.28\%$ and 0.14% for the 300 K and 1000 K solutions. An important measure for these fluids is the time scale characterizing the chain unraveling process in an elongational flow [33], referred to as the elongational relaxation time (τ_E). We show in the Supplemental Material [34] that, beyond a critical strain rate ($\dot{\epsilon} \gtrsim \tau_E^{-1}$), the extensional viscosity of these solutions increases dramatically. This critical strain rate varies with the molecular weight and concentration [38–40]. It can easily be exceeded in the final stages of atomization in which capillary-driven pinch off processes lead to thin threads $[R(t) \to 0]$ and extremely high values of the local strain rate $\dot{\epsilon}(t) \sim -2\dot{R}/R(t)$. Thus, the enhanced extensional viscosity of a dilute solution will inhibit the capillary-driven thinning of liquid ligaments and may retard the subsequent atomization process.

To illustrate the fragmentation-coalescence process, we show, in Fig. 2(a), the break up of a single fluid filament (drawn rapidly out of a bath of fluid) into a set of droplets. This process is a capillary-dominated phenomenon between the neighboring liquid blobs that initially emerge on the ligament (shown as magenta circles). The geometry of the precursor liquid thread sets the size distribution of these initial blobs. Knowing that the geometry of the initial ligaments determines the final droplet size distribution in a Newtonian spray [7], we analyzed the droplet size distribution for the Newtonian solvent and all four viscoelastic solutions, gathering a set of almost five thousand droplets for each liquid. In Fig. 2(b), we show the PDF for the Newtonian solvent and for all four viscoelastic test fluids (corresponding to $0.2 \leq \mathrm{De} \leq 10$). Remarkably, the viscoelastic solutions show a universal behavior which is independent of both the molecular weight and the concentration of the dissolved polymer. All show a size distribution that is well described by a Gamma distribution; however, the polymer solutions have a much broader size distribution. The viscoelastic data are characterized by a Gamma distribution with $n = 4$ (compared to $n = 6$ for the Newtonian solvent). As in the Newtonian case, the corresponding best fit from a log-normal distribution fails to correctly capture the probability distributions at large sizes (identical trends are obtained in atomization tests with paint "resins"; see the Supplemental Material [34] for details).

For Newtonian fluids, Villermaux and co-workers [10,11,41] show that the value of n characterizing the final Gamma distribution is determined by the smoothness of the initial ligaments when they detach from the core liquid jet. The index n is a measure of the corrugation in the initial ligaments which the final spray of droplets inherits in its size distribution. They show that the value of n can be predicted just by the geometrical shape of the initial ligament

$$n \equiv \langle d \rangle_0^2 / (\langle d^2 \rangle_0 - \langle d \rangle_0^2), \tag{2}$$

in which $\langle \ldots \rangle$ indicates a number average and $d_i = 2r_i$ are the diameters of the protoblobs that one can fit in the profile of the ligament at the instant of pinch-off from the core liquid jet [shown with magenta circles in Fig. 2(a) and by the dashed circles in Fig. 3(c) below]. A very uniform ligament at $t = 0$ leads to a very large value of n and, consequently, a very narrow final droplet size distribution. By contrast, a highly corrugated initial ligament in which fluctuations in the local blob diameters are large leads to smaller values of n and broader size distributions.

The universal decrease in the values of n for viscoelastic sprays arises from the high extensional viscosity which changes the geometry of initial ligaments from smooth to more corrugated shapes. Tracking the geometry of ligaments in atomization is an ongoing visualization challenge. A much simpler test is an axial "step-strain" test, consisting

TABLE I. Properties of the viscoelastic test fluids.

Mw	c/c^*	$\eta_0[\mathrm{mPa \cdot s}]$	$\tau_E[\mu s]$	L	De	Oh
300 K	(0.036, 0.36)	(3.21, 3.32)	(60, 360)	27	(0.2, 1.3)	0.04
1000 K	(0.07, 0.37)	(3.22, 3.31)	(996, 2800)	50	(3.6, 10)	0.04

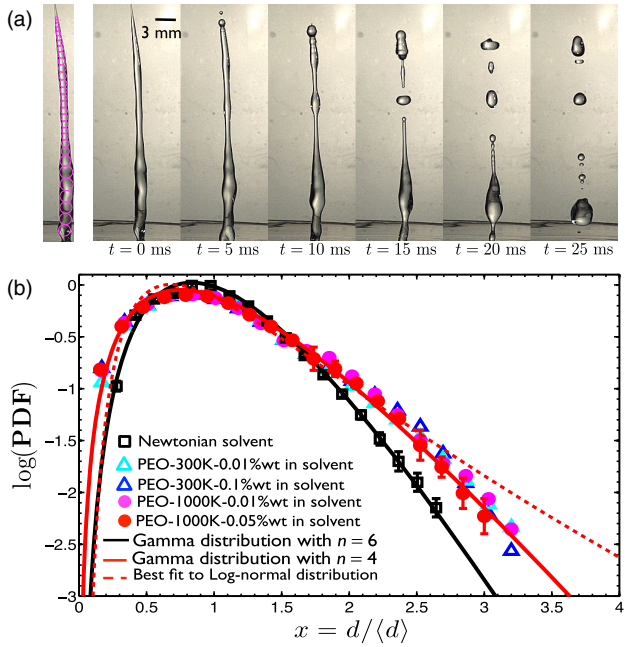

FIG. 2. (a) Images from the fragmentation process for a Newtonian ligament (with the index $n = 8$). The coalescence of the neighboring blobs in the ligament at $t = 0$ (magenta circles on the left image) results in the final distribution of droplet sizes at $t = 25$ ms. (b) Droplet size distributions for all tested liquids in the air-assisted atomization process. For each fluid we specify the values of Ohnesorge and Deborah number, $\{\mathrm{Oh}, \mathrm{De}\}$:(black squares)$\{\mathrm{Oh} = 0.04, \mathrm{De} = 0\}$, (cyan triangles)$\{0.04, 0.2\}$, (blue triangles)$\{0.04, 1.3\}$, (magenta circles)$\{0.04, 3.6\}$, (red circles) $\{0.04, 10.0\}$. Solid lines are Gamma distributions for $n = 6$ (black) and $n = 4$ (red).

of a liquid sample confined between two cylindrical plates which are then separated at relatively high stretch rates. The dynamics of fragmentation can be properly replicated through such a test [41], and we use this geometry to study the configuration of viscoelastic ligaments at short times after separation from the liquid core. Figure 3(a) shows a montage of images for the PEO 300 K solution ($c/c^* = 0.36$). The fast dynamics of the initial capillary thinning forms capillary waves on the ligament as soon as it separates from the liquid cusps that develop due to the strong squeezing flow in the necks of the ligaments. In contrast to Newtonian liquids (where capillary thinning rapidly leads to droplet pinch off), in viscoelastic ligaments, the squeezing flow leads to a localized high strain rate in the neck and the elongating liquid elements resist pinch-off due to the enhanced extensional viscosity [17]. This localized elongational flow leads to a highly corrugated beads-on-a-string morphology [17,18,42,43]. The viscoelastic ligament in Fig. 3(c) has a more corrugated shape compared to the corresponding Newtonian case, and axial variations in the diameter of local blobs $d_i(z)$ are much larger than the corresponding Newtonian case. As shown in Fig. 3(b), the distribution of blob sizes can be determined by identifying space filling spheres located at positions where the wavy profile is locally a peak or a trough; thus, the radius of the ith blob is $r_i = r_0 + \xi_i$ in which r_0 is the radius of the undisturbed ligament, and ξ_i is the deviation of the peak ($\xi_i > 0$) or trough ($\xi_i < 0$). The resulting values of n are calculated using Eq. (2) and show a drastic decrease from $n \simeq 51$ for the Newtonian solvent to $n \simeq 4$ for the viscoelastic solution [44]. These changes in the distribution of corrugations are triggered in all of the viscoelastic fluids, regardless of either polymer concentration or molecular weight, because of the divergent nature of the local strain rate $\dot{\epsilon}(t)$ in the necking filament, which ultimately induces coil-stretch transition in all of the polymer solutions studied.

To understand the universal saturation in the atomization behavior ($n \to 4$), we investigate the origins of the corrugations. Interfacial disturbances on a ligament can be generated from a combination of capillary and shear instabilities. The resulting ligament profile deviates from purely cylindrical $r(z) = r_0$ by wavelike modulations of an arbitrary form [45,46] that change the distribution of the initial blobs in a ligament from a monodisperse distribution ($r_i = r_0$ and $n \to \infty$) on a perfectly smooth cylinder to broader distributions ($r_i = r_0 + \xi_i$) with progressively

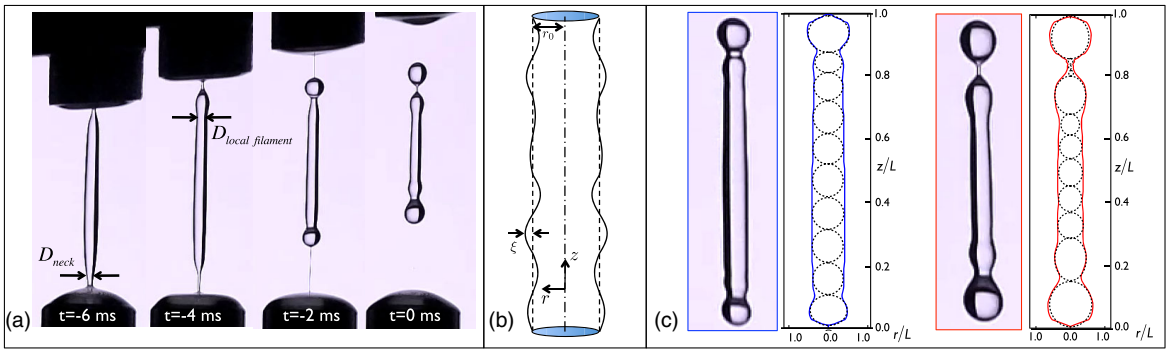

FIG. 3. (a) Sudden stretch experiment for a viscoelastic solution at high strain rates ($\bar{\dot{\epsilon}} \simeq 120\ \mathrm{s}^{-1}$). (b) Schematics of a cylindrical ligament with initial radius r_0 corrugated by perturbations with similar wavelengths but varying amplitude ξ. (c) Ligament profiles for the Newtonian solvent (blue curve) compared with the viscoelastic solution (red curve) at the breaking point from the liquid hemispherical reservoirs ($t = 0$). The dashed circles indicate the local protoblobs inside each ligament.

lower values of n. The amplitude of the perturbations can not exceed the radius of the ligament (thus, $-r_0 \le \xi_i \le r_0$), and due to the random wavy nature of corrugations, we also expect $\langle \xi_i \rangle = 0$. Upon substituting these expressions, Eq. (2) simplifies to $n = r_0^2/\langle \xi_i^2 \rangle$. The geometrical constraint $|\xi_i| \le r_0$ gives a minimum value of $n_{\min} = 1$. To reach such a small value of $n_{\min} = 1$, the number of protoblobs in the ligament has to vary as the corrugations develop prior to the onset of fragmentation or coalescence [$t = 0$ in Fig. 3(a)]. Although this is mathematically possible, we have never observed anything less than $n_{\min} = 4$, which suggests that the number of protoblobs N is constant during the development of corrugations, not only in the sudden stretch test, but also in all our other atomization geometries. Assuming a constant number of protoblobs prior to the onset of coalescence, we consider conservation of volume inside the isolated ligament and impose an additional constraint on the third moment of the blob radii distribution, giving $\langle r_i^3 \rangle \le (3/2) r_0^3$ [47]. Substituting $r_i = r_0 + \xi_i$, this new constraint can be simplified to $3 r_0 \langle \xi_i^2 \rangle + \langle \xi_i^3 \rangle \le (1/2) r_0^3$. By introducing a new dimensionless amplitude parameter ($-1 \le \alpha_i \equiv \xi_i / r_0 \le 1$), the constraints on the initial blob size distributions can be rewritten compactly in the form:

$$\langle \alpha_i \rangle = 0\text{: random wavy nature of corrugations,} \quad (3a)$$

$$3\langle \alpha_i^2 \rangle + \langle \alpha_i^3 \rangle \le 1/2\text{: conservation of volume.} \quad (3b)$$

Recognizing that $n = 1/\langle \alpha_i^2 \rangle$, the last constraint in Eq. (3) can be rewritten as $\min\{6/(1 - 2\langle \alpha_i^3 \rangle)\} \le n$. The minimum value of the function $6/(1 - 2\langle \alpha_i^3 \rangle)$ will, thus, set the minimum for the index n. This minimum is obviously achieved when $\langle \alpha_i^3 \rangle$ attains its most negative value, also subject to Eq. (3a). Introducing a simple variable transformation of $\alpha_i = \cos(\theta_i)$, we can rewrite $\langle \alpha_i^3 \rangle = \langle \cos^3(\theta_i) \rangle = (1/4)\langle [\cos(3\theta_i) + 3\cos(\theta_i)] \rangle$. Using the first condition in Eq. (3), this reduces to $\langle \alpha_i^3 \rangle = (1/4)\langle \cos(3\theta_i) \rangle$, which lies between $-1/4$ and $+1/4$. Thus, it is clear that the exponent n can not be lower than a minimum value of $n_{\min} = 6/(1 - 2\langle \alpha_i^3 \rangle) = 4$. This proof is consistent with earlier scaling arguments that the geometric roughness of the initial ligaments will reach a saturation limit which is set by geometry and volume constraints [48].

We also performed similar tests in two other ligament-meditated fragmentation processes. First, we studied drop impact experiments in which a liquid drop ($D \sim 4$ mm) impacts on a small target of comparable diameter at high Weber numbers ($\mathrm{We} = \rho V^2 D/\sigma \gtrsim 400$). As shown in Fig. 4(a), following impact, a curtain of liquid expands outwards from the target and finally bursts into a set of droplets. We also considered jet impact atomization consisting of two identical liquid jets that collide at a fixed angle [shown in Figs. 4(b)–4(i)] [49]. Villermaux and co-workers [50,51] have shown, for Newtonian fluids, that ligament-meditated fragmentation also occurs in these types of atomization. Droplet visualization shows that viscoelasticity again leads to larger numbers of both big and small drops [Figs. 4(a-ii) and 4(b-iii)], whereas in the Newtonian case, the drop size distributions is narrower. A summary of the measured breadth of the droplet size distributions for these two new tests, along with data from air-assisted atomization is shown in Fig. 4(c). We show the values of the Sauter mean diameter ($\mathrm{SMD} \equiv \sum d_i^3 / \sum d_i^2$) computed directly from the measured droplet size distributions and normalized by the average diameter ($\langle d \rangle$) versus the measured values of n obtained from fitting Gamma distributions to the measured PDF for each experiment (each consisting of $N \ge 5000$ droplets). For a Gamma distribution $\mathrm{SMD}/\langle d \rangle = 1 + 2/n$, and the solid line in Fig. 4(c) shows this analytical prediction compared with the experimental measurements. In all three flows, the addition of viscoelasticity decreases the value of n from that observed in the same flow for a Newtonian fluid. Even for weakly elastic polymer solutions with relaxation times as low as 60 μs, the size distributions universally approach $n = 4$ in each flow.

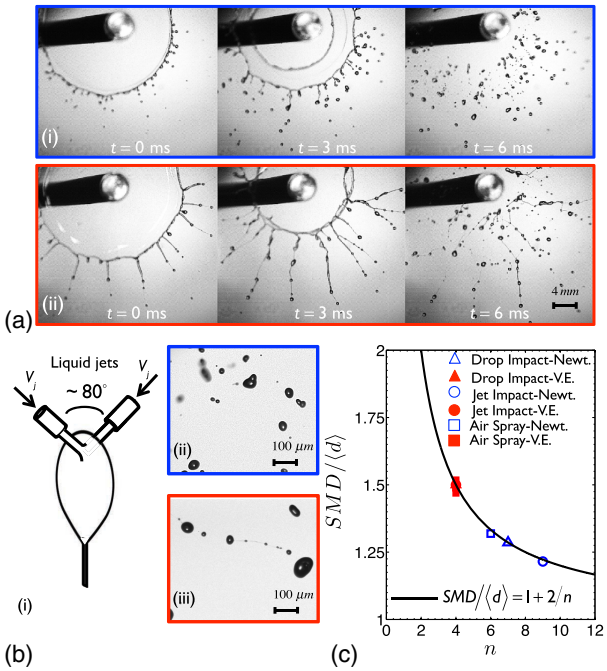

FIG. 4. (a) Fragmentation after drop impact on a small target. Montage of images for (i) the Newtonian solvent and (ii) a polymer solution (PEO 300 K). (b) Snapshots of the droplets captured after fragmentation by jet impact atomization (i) for (ii) the Newtonian solvent and (iii) viscoelastic solution. (c) Summary of the measured values of the dispersity $\mathrm{SMD}/\langle d \rangle$ in three different fragmentation processes for both the Newtonian solvent (blue) and the viscoelastic (denoted V.E.) solutions (red) compared with the theoretical prediction (solid line).

Our results indicate that this viscoelastic broadening mechanism is driven by the local dynamics of the strong extensional flow in the filament necks. Although viscoelasticity monotonically increases the average droplet size $\langle d \rangle$ [27], the distribution of sizes about the mean value are uniquely determined by a broad Gamma distribution with $n = 4$. This geometrical limit is triggered by the enhanced elongational viscosity experienced during the capillary pinch-off process (provided that the concentration of the microstructure is above the "infinite dilution limit" [52]) and results in highly corrugated ligaments. The final size distribution is constrained entirely due to geometry and conservation of volume. Recognizing this bound is essential in many processes such as emulsification, spray painting, and even biological processes such as pathogen transfer resulting from violent expiration [53].

B. K. and G. H. M. thank the Dupont-MIT-Alliance (DMA) and Axalta Coating Systems for their financial support. B. K. and G. H. M. also thank Emmanuel Villermaux for sharing his insightful ideas on the fragmentation process via personal communications. B. K. also thanks William H. Bowman from Axalta Coating Systems.

*bavand@mit.edu

[1] M.-H. Wei, B. Li, R. L. A. David, S. C. Jones, V. Sarohia, J. A. Schmitigal, and J. A. Kornfield, Science **350**, 72 (2015).
[2] M. Jaffe and S. Allam, Science **350**, 32 (2015).
[3] A. H. Lefebvre, *Atomization and Sprays* (Hemisphere Publishing Corporation, New York, 1989), p. 421.
[4] A. Déchelette, E. Babinsky, and P. E. Sojka, in *Handbook of Atomization and Sprays SE—23*, edited by N. Ashgriz (Springer, New York, 2011), pp. 479–495.
[5] Lucretius, *On the Nature of Things* (W. W. Norton & Company, New York, 2011), p. 177.
[6] D. C. Blanchard, *From Raindrops to Volcanoes: Adventrues with Sea Surface Meteorology* (Doubleday Anchor, Garden City, NY, 1967).
[7] E. Villermaux, Annu. Rev. Fluid Mech. **39**, 419 (2007).
[8] H. M. Gonnermann, Annu. Rev. Earth Planet Sci. **43**, 431 (2015).
[9] E. Villermaux and J. Duplat, Phys. Rev. Lett. **91**, 184501 (2003).
[10] E. Villermaux, P. Marmottant, and J. Duplat, Phys. Rev. Lett. **92**, 074501 (2004).
[11] E. Villermaux and B. Bossa, Nat. Phys. **5**, 697 (2009).
[12] M. A. Gorokhovski and V. L. Saveliev, Phys. Fluids **15**, 184 (2003).
[13] R. D. Cohen, Proc. R. Soc. A **435**, 483 (1991).
[14] M. Von Smoluchowski, Z. Phys. Chem. **92**, 129 (1917).
[15] Provided a narrow ligament size distribution, the final droplet size distribution in a spray has a similar form to Eq. (1). However, as noted by Marmottant and Villermaux [16], for Newtonian liquids, changing the momentum of the air stream can broaden the ligament size distributions and change the corrugation level for the individual ligaments. Thus, the final size distribution at certain air speeds may be closer to the form of an incomplete Gamma function [16]. Importantly, however, this will have an exponential tail with the same value of the index n.
[16] P. Marmottant and E. Villermaux, J. Fluid Mech. **498**, 73 (2004).
[17] C. Wagner, Y. Amarouchene, D. Bonn, and J. Eggers, Phys. Rev. Lett. **95**, 164504 (2005).
[18] R. Sattler, C. Wagner, and J. Eggers, Phys. Rev. Lett. **100**, 164502 (2008).
[19] H. Lhuissier, B. Néel, and L. Limat, Phys. Rev. Lett. **113**, 194502 (2014).
[20] J. W. Hoyt, J. J. Taylor, and C. D. Runge, J. Fluid Mech. **63**, 635 (1974).
[21] J. E. Matta, Army Armament Research and Development Command, Aberdeen Proving Ground, MD. Chemical Systems Lab. 1, Technical Report, May 1979–Apr. 1980, 1981.
[22] J. E. Matta and R. P. Tytus, J. Appl. Polym. Sci. **27**, 397 (1982).
[23] J. E. Matta, R. P. Tytus, and J. L. Harris, Chem. Eng. Commun. **19**, 191 (1983).
[24] J. Ferguson, N. E. Hudson, and B. C. H. Warren, J. Non-Newtonian Fluid Mech. **44**, 37 (1992).
[25] Z. Ergungor, C. W. Manke, and E. Gulari, J. Non-Newtonian Fluid Mech. **97**, 159 (2001).
[26] L. M. Walker and Y. Christanti, Atom. Sprays **16**, 777 (2006).
[27] B. Keshavarz, V. Sharma, E. C. Houze, M. R. Koerner, J. R. Moore, P. M. Cotts, P. Threlfall-Holmes, and G. H. McKinley, J. Non-Newtonian Fluid Mech. **222**, 171 (2015).
[28] A. A. Avdienko, J. Eng. Phys. Thermophys. **66**, 149 (1994).
[29] E. Babinsky and P. E. Sojka, Atom. Sprays **11**, 22 (2001).
[30] J. W. Hoyt and J. J. Taylor, Phys. Fluids **20**, S253 (1977).
[31] D. F. James, Annu. Rev. Fluid Mech. **41**, 129 (2009).
[32] R. B. Bird, R. C. Armstrong, and O. Hassager, *Dynamics of Polymeric Liquids*, 2nd ed. (John Wiley & Sons, New York, 1987), Vol. 1.
[33] P. S. Doyle, E. S. Shaqfeh, G. H. McKinley, and S. H. Spiegelberg, J. Non-Newtonian Fluid Mech. **76**, 79 (1998).
[34] See Supplemental Material at http://link.aps.org/supplemental/10.1103/PhysRevLett.117.154502 for extra information on the rheology and fragmentation tests for different liquids, which includes Refs. [35–37].
[35] L. E. Rodd, T. P. Scott, J. J. Cooper-White, and G. H. McKinley, Applied Rheology **15**, 12 (2005).
[36] L. E. Rodd, T. P. Scott, D. V. Boger, J. J. Cooper-White, and G. H. McKinley, J. Non-Newtonian Fluid Mech. **129**, 1 (2005).
[37] G. Magnus, Philos. Mag. **11**, 178 (1856).
[38] P. G. De Gennes, J. Chem. Phys. **60**, 5030 (1974).
[39] T. T. Perkins, D. E. Smith, R. G. Larson, and S. Chu, Science **268**, 83 (1995).
[40] S. J. Haward, M. S. N. Oliveira, M. A. Alves, and G. H. McKinley, Phys. Rev. Lett. **109**, 128301 (2012).
[41] P. Marmottant and E. Villermaux, Phys. Fluids **16**, 2732 (2004).
[42] M. S. N. Oliveira and G. H. McKinley, Phys. Fluids **17**, 071704 (2005).
[43] P. P. Bhat, S. Appathurai, M. T. Harris, M. Pasquali, G. H. McKinley, and O. A. Basaran, Nat. Phys. **6**, 625 (2010).

[44] Obviously, the fact that aerodynamic effects from the surrounding annular air flow do not appear in the sudden stretch test results in the Newtonian ligament having a very smooth initial profile and a higher value of n compared to a real fragmentation processes.
[45] L. Rayleigh, Philos. Mag. **10**, 73 (1880).
[46] M. S. Longuet-Higgins, J. Mar. Res. **11**, 245 (1952).
[47] The $3/2$ factor comes from the fact that the liquid volume in the initially undisturbed ligament is the volume inside a cylinder with radius r_0 which is $3/2$ times higher than the sum of identical neighboring spherical blobs with radius r_0. This $3/2$ factor was originally discovered by Archimedes.
[48] J. Eggers and E. Villermaux, Rep. Prog. Phys. **71**, 036601 (2008).
[49] G. Magnus, Ann. Phys. (Berlin) **171**, 1 (1855).
[50] N. Bremond and E. Villermaux, J. Fluid Mech. **549**, 273 (2006).
[51] E. Villermaux and B. Bossa, J. Fluid Mech. **668**, 412 (2011).
[52] C. Clasen, J. P. Plog, W. M. Kulicke, M. Owens, C. Macosko, L. E. Scriven, M. Verani, and G. H. McKinley, J. Rheol. **50**, 849 (2006).
[53] L. Bourouiba, E. Dehandschoewercker, and J. Bush, J. Fluid Mech. **745**, 537 (2014).